Author(s): Pérez de Rada, A.; Cano-Ott, D.; Martínez, T.; Alcayne, V.; Mendoza, E.; Plaza, J.; Sanchez-Caballero, A.; Villamarín, D.; Äystö, J.; Jokinen, A.; Kankainen, A.; Penttilä, H.; Rinta-Antila, S.; Agramunt, J.; Algora, A.; Domingo-Pardo, C.; Lerendegui-Marco, J.; Taín, J.L.; Banerjee, K.; Bhattacharya, C.; Roy, P.; Calviño, F.; Cortés, G.; Delafosse, C.; Matea, I.; Benito, J.; Alhomaidhi, S.; Mistry, A.K.

Title: β-delayed neutron spectroscopy of 85,86As with MONSTER

Year: 2023

Version: Published version

β-delayed neutron spectroscopy of ^{85,86}As with MONSTER

A. Pérez de Rada[1,*], *D.* Cano-Ott[1], *T.* Martínez[1], *V.* Alcayne[1], *E.* Mendoza[1], *J.* Plaza[1], *A.* Sanchez-Caballero[1], *D.* Villamarín[1], *J.* Äystö[2], *A.* Jokinen[2], *A.* Kankainen[2], *H.* Penttilä[2], *S.* Rinta-Antila[2], *J.* Agramunt[3], *A.* Algora[3], *C.* Domingo-Pardo[3], *J.* Lerendegui-Marco[3,8], *J. L.* Taín[3], *K.* Banerjee[4,5], *C.* Bhattacharya[4,5], *P.* Roy[4,5], *F.* Calviño[6], *G.* Cortés[6], *C.* Delafosse[2,7], *I.* Matea[7], *J.* Benito[9], *S.* Alhomaidhi[10,11], and *A. K.* Mistry[10,11]

[1]Centro de Investigaciones Energéticas, Medioambientales y Tecnológicas (CIEMAT), E-28040 Madrid, Spain
[2]JYFL, The Accelerator Laboratory of the Department of Physics, University of Jyväskylä, FI-40014 Jyväskylä, Finland
[3]Instituto de Física Corpuscular (IFIC), CSIC-Universidad de Valencia, E-46071 Valencia, Spain
[4]Variable Energy Cyclotron Centre (VECC), IN-700064 Kolkata, India
[5]Homi Bhabha National Institute (HBNI), IN-400094 Anushakti Nagar, Mumbai, India
[6]Universitat Politècnica de Catalunya (UPC), Departament de Física, E-08034 Barcelona, Spain
[7]IJCLab, Université Paris-Saclay, CNRS/IN2P3, FR-91405 Orsay Cedex, France
[8]Universidad de Sevilla (US), Facultad de Física, E-41012 Sevilla, Spain
[9]Universidad Complutense de Madrid (UCM), Grupo de Física Nuclear, E-28040 Madrid, Spain
[10]Institut für Kernphysik, Technische Universität Darmstadt, D-64289 Darmstadt, Germany
[11]GSI Helmholtzzentrum für Schwerionenforschung, D-64291 Darmstadt, Germany

Abstract. The β-delayed neutron emission in the ^{85,86}As β-decays has been measured at the IGISOL facility of the Accelerator Laboratory of the University of Jyväskylä (JYFL-ACCLAB). The complete β-decays have been studied with a complex setup that consists of a plastic scintillator, the **MO**dular **N**eutron time-of-flight **S**pectrome**TER** (MONSTER), and two types of γ-ray detectors—an HPGe clover and four $LaBr_3$ crystals. The β-delayed neutron energy distributions have been determined by unfolding the TOF spectra with an innovative methodology based on the iterative Bayesian unfolding method and accurate Monte Carlo simulations.

1 Introduction

The field of β-delayed neutrons has experienced an increased activity during the last decades [1] thanks to the advances in nuclear experimental techniques and radioactive ion beam (RIB) facilities producing increased yields of neutron-rich isotopes. Properties from individual precursors like the emission probability, β-feeding, and energy spectrum are being measured with advanced neutron detectors [2–4], digital data acquisition (DAQ) systems [5], and high intensity RIBs [6–9].

In this paper, the results obtained in the measurement at the IGISOL facility of the Accelerator Laboratory of the University of Jyväskylä (JYFL-ACCLAB) on the β-delayed neutron energy distributions following the ^{85,86}As β-decays are reported. Some relevant properties of the β-decays of interest are presented in Table 1 [10].

Table 1. Relevant properties of the β-decays.

Isotope	$T_{1/2}$ (s)	Q_β (keV)	$Q_{\beta n}$ (keV)	P_n (%)
^{85}As	2.021	9224.5	4687.2	59.4
^{86}As	0.945	11541.0	5380.2	35.5

*e-mail: alberto.rada@ciemat.es

2 Experimental setup

The ^{85,86}As isotopes were produced by proton-induced fission reactions in a ^{nat}U target. In each case, the isobars were separated from the bulk of fission products by the IGISOL dipole magnet with resolution $M/\Delta M = 500$ [9] and implanted on a movable tape inside of the β-detector.

The β-detector [11] consisted of a BC408 cup-like shaped plastic detector wrapped with reflector foil and coupled to an R5924-70 PMT from Hamamatsu. The detector was placed inside the vacuum pipe and had a 10 mm aperture on the side of the detector cup that allowed for the implantation on the tape to take place.

The emitted β-delayed neutrons were detected with the **MO**dular **N**eutron time-of-flight **S**pectrome**TER** (MONSTER) [4, 12]. MONSTER consists of cylindrical cells of 200 mm diameter and 50 mm height, filled with either BC501A or EJ301 scintillating liquid. Each cell was coupled through a light guide of 31 mm thickness to either a R4144 or R11833 PMT from Hamamatsu. For this experiment, 48 cells arranged in two different setups, with 30 and 18 cells at 2 and 1.5 m flight paths, respectively, were used.

The signals from the β-detector and MONSTER were used as the start and stop signals, respectively, to measure the neutrons' time-of-flight (TOF). A picture of the whole ensemble can be seen in Figure 1.

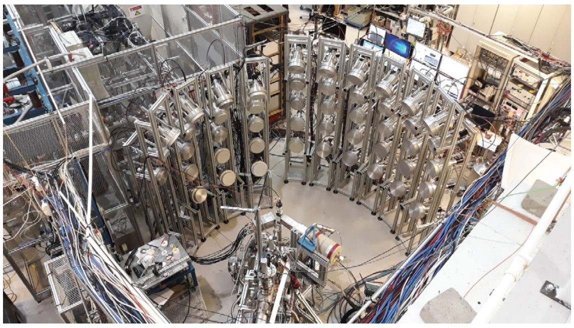

Figure 1. Experimental setup mounted at JYFL-ACCLAB.

All the detector signals were registered with a custom digital DAQ system developed at CIEMAT based on ADQ14DC digitizers from Teledyne SP Devices with 14 bits vertical resolution, 1 GSample/s sampling rate, and 4 channels [5]. The complete setup required 60 channels. The system integrates custom pulse shape analysis software also developed at CIEMAT to analyze the registered signals online. The used pulse shape analysis routines did not add any dead time to the measurement.

The data was collected in cycles of implantation and decay adapted to the half-lives of the isotopes involved for maximizing the activity of the neutron emitters with respect to the other implanted isobars. During the cycle, the ion beam was switched on and off by electrostatic deflection at the switchyard of the IGISOL beam line. The cycle also included an initial time interval for background measurement and a final time interval for removal of the long-lived activity of the decay products.

3 Efficiency characterization

The β-detector efficiency was determined experimentally at two different endpoint energy values from the ^{92}Sr into ^{92}Y β-decay through the β-γ coincidence method using the HPGe and $LaBr_3$ detectors. The Monte Carlo simulations were used for extending the detector efficiency as a function of the endpoint energy and for estimating the detection threshold of 260 keV. The results of the efficiency calculation and the comparison with the experimental data are shown in Figure 2.

The MONSTER neutron detection efficiency was determined through Monte Carlo simulations and validated with the data from a measurement with a 1.00 ± 0.15 GBq ^{252}Cf source. The γ-rays from the spontaneous fission of ^{252}Cf detected in the $LaBr_3$ detectors served for establishing a TOF between the emission and the detection of the spontaneous fission neutrons. Neutron signals in MONSTER were selected by performing pulse shape discrimination, allowing for a reduction of the background due to γ-rays of one order of magnitude. The response of MONSTER to different neutron energies was obtained by setting different cuts in the γ-neutron TOF spectrum. The Monte Carlo simulations were performed with the light output response obtained from previous calibrations with monochromatic energy neutron beams [12]. There is an excellent agreement between the experimental values and the Monte Carlo simulations of the MONSTER arrays for the two different flight paths, as shown in Figure 3.

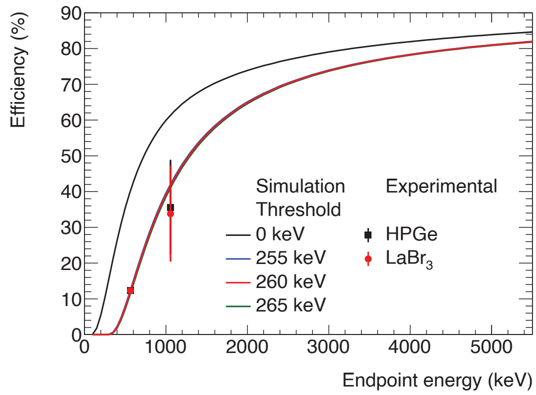

Figure 2. β-efficiency determined from the ^{92}Sr into ^{92}Y β-decay and comparison with Monte Carlo simulations.

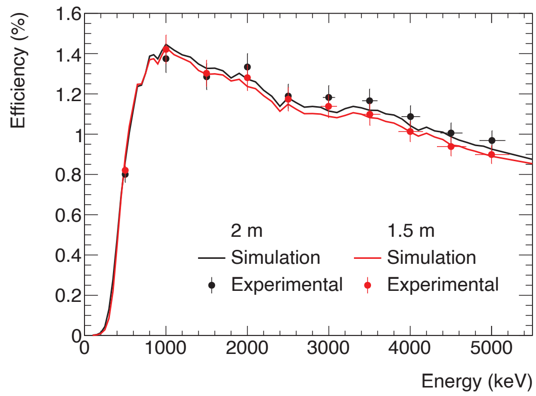

Figure 3. Total neutron detection efficiency for both MONSTER arrays determined from the ^{252}Cf source and comparison with Monte Carlo simulations.

4 Data analysis and results

4.1 β-activity distributions

The time evolution of the β-activity during each cycle due to all isotopes in the decay chain is governed by the Bateman equations. The experimental β-activity distribution is fitted with a function based on the generic solution given in [13] that describes the contribution of each of the isotopes involved in the decay chain:

$$A(t) = \sum_{i=1}^{n} \overline{\epsilon_i} \lambda_i N_i(t), \quad (1)$$

where $\overline{\epsilon_i}$ is the average efficiency to detect a β-particle coming from the β-decay of the i-th member of the chain, λ_i is the decay constant of the i-th member of the chain, and $N_i(t)$ is the number of nuclei of the i-th member of the chain given by the solution of the Bateman equations, which depends on the respective implantation rate R_i.

The experimental β-activity distributions for both decays, together with the total fits and the individual contributions, can be seen in Figure 4. The measurement cycle in the case of ^{86}As was shorter in order to maximize its contribution with respect to the other implanted isobars.

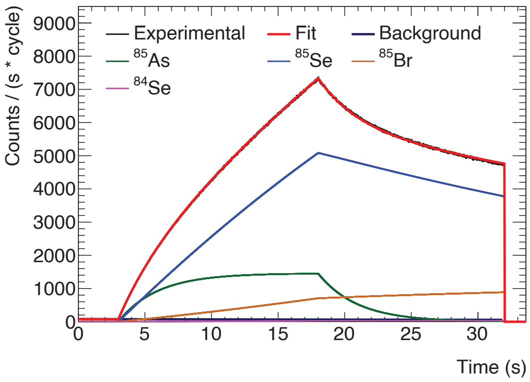

(a) ^{85}As

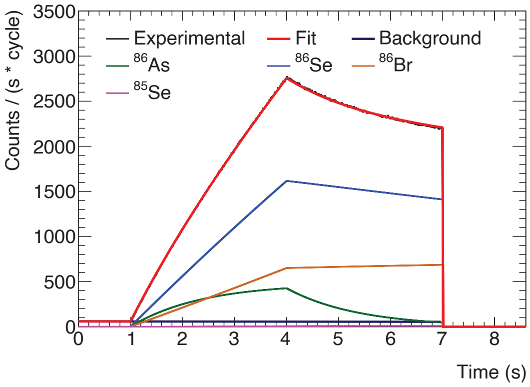

(b) ^{86}As

Figure 4. Time evolution of the β-activity distributions and the corresponding fits, including individual contributions.

The results of the fits are presented in Table 2. The other values that are in the table are the calculated average detection efficiencies as well as the total number of decays of each of the isotopes. The average detection efficiencies for each of the β-decays were calculated through Monte Carlo simulations using available data.

4.2 TOF spectra unfolding

An innovative analysis procedure based on the iterative Bayesian unfolding method [14] was developed to obtain the neutron energy distributions from the measured TOF spectra [15].

Assuming an initial probability distribution of independent causes (neutron energies) and the probability of each of the causes to produce specific effects (TOF spectrum), the conditional probability of a specific effect (E_j) being due to a certain cause (C_i) is given by:

Table 2. Results of the fit to the β-activity curve, along with the calculated average efficiencies and the total number of decays.

Isotope	$\overline{\epsilon}$ (%)	R (ions/s)	Total decays ($\times 10^6$)
^{85}As	80.8 ± 4.0	1800 ± 100	48 ± 3
^{85}Se	76.0 ± 3.8	23300 ± 900	239 ± 9
^{85}Br	69.7 ± 3.5	13900 ± 2500	42 ± 5
^{84}Se	55.1 ± 2.8	0 ± 0	1.8 ± 0.1
^{86}As	83.5 ± 4.2	570 ± 40	12.7 ± 0.8
^{86}Se	72.9 ± 3.6	16100 ± 400	74 ± 2
^{86}Br	77.5 ± 3.9	21500 ± 2100	30 ± 3
^{85}Se	76.0 ± 3.8	0 ± 0	0.32 ± 0.02

$$P(C_i|E_j) = \frac{P(E_j|C_i)P_0(C_i)}{\sum_{l=1}^{n_c} P(E_j|C_l)P_0(C_l)}. \tag{2}$$

The conditional probability $P(E_j|C_i)$ is the response matrix of the detection system and can be estimated through Monte Carlo simulations. The construction of the response matrix is crucial to achieve an accurate result. The built response matrices covered the whole energy range up to the $Q_{\beta n}$ values of the decays in intervals chosen according to the energy resolution of the system, and included an extra flat contribution to account for the γ-ray background.

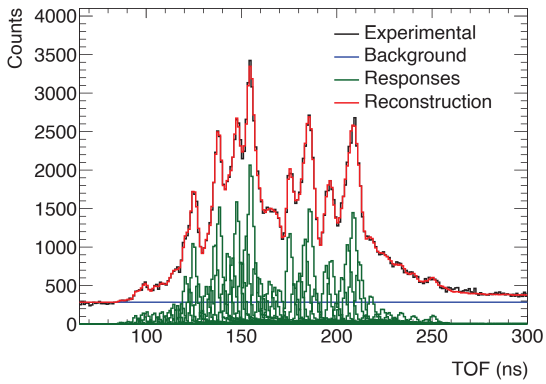

(a) ^{85}As

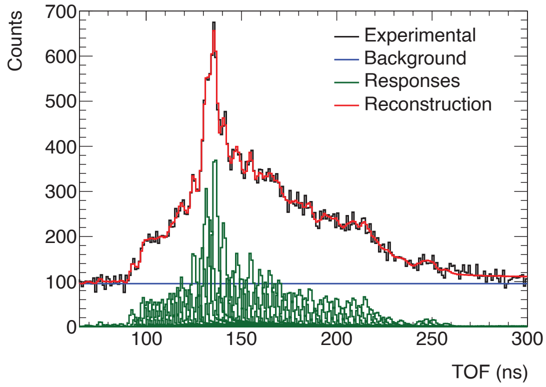

(b) ^{86}As

Figure 5. Experimental TOF spectra together with the reconstructions and individual causes' contributions.

The measured experimental TOF spectra for both decays and their reconstructions can be seen in Figure 5 for the MONSTER array at 2 m.

Finally, the neutron energy distributions obtained with both MONSTER arrays are presented in Figure 6. The agreement of the results obtained with both arrays is excellent within their energy resolution. The obtained results are also compared to existing data [10, 16]. The existing data has been rebinned to the binning of the results of this work. Also, the obtained energy distributions have been scaled so that the intensities over the experimental threshold of around 300 keV are equal to those of the existing data. The results obtained for ^{85}As are in excellent agreement with evaluations, which include experimental data obtained by the Mainz group and are supplemented with theoretical calculations. It's worth noting that no neutron intensity over around 3 MeV, which is predicted by calculations, is observed. No previous experimental data has been found for ^{86}As on the bibliography. The results of this work are in reasonable agreement with evaluations.

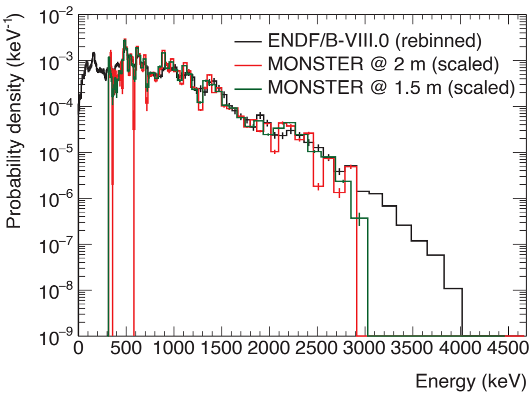

(a) ^{85}As

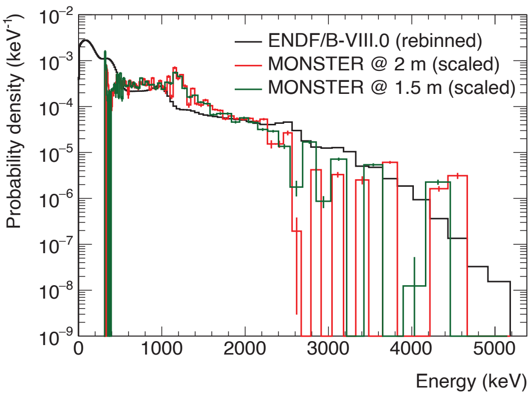

(b) ^{86}As

Figure 6. Neutron energy distributions obtained with both MONSTER arrays and compared to existing data.

5 Summary

This work is a successful commissioning and measurement with MONSTER, a neutron TOF spectrometer with excellent neutron/γ-ray discrimination capabilities and neutron energy resolution.

The efficiency of the different detectors has been obtained experimentally and reproduced with accurate Monte Carlo simulations.

An innovative analysis methodology has been developed. It is based on the fit of the β-activity curves with the Bateman equations and on the unfolding of the neutron TOF spectra with the iterative Bayesian unfolding method based on accurate Monte Carlo simulations.

The β-delayed neutron energy spectrum of ^{85}As has been procured. This result is in excellent agreement with previous experimental data and evaluations, and serves as the validation of the developed analysis methodology.

Lastly, the β-delayed neutron energy spectrum of ^{86}As has been procured for the first time. The obtained energy distribution is in reasonable agreement with evaluations.

References

[1] P. Dimitriou *et al.*, Nucl. Data Sheets, **173**, 144-238 (2021)
[2] A. Buţă *et al.*, Nucl. Instrum. and Methods A, **455**, 412-423 (2000)
[3] W. A. Peters *et al.* Nucl. Instrum. and Methods A, **836**, 122-133 (2016)
[4] A. R. García *et al.*, JINST, **7**, C05012 (2012)
[5] D. Villamarín *et al.*, Design of a high performance Digital data AcquIsition SYstem (DAISY) for innovative nuclear experiments. Submitted for publication
[6] P. Spiller *et al.*, Nucl. Instrum. and Methods A, **561**, 305-309 (2006)
[7] H. Okuno *et al.*, Prog. Theor. Exp. Phys., 03C002 (2012)
[8] R. Catherall *et al.*, Nucl. Instrum. and Methods B, **317**, 204-207 (2013)
[9] I. D. Moore *et al.*, Nucl. Instrum. and Methods B, **317**, 208-213 (2013)
[10] D. A. Brown *et al.*, Nucl. Data Sheets, **148**, 1-142 (2018)
[11] Z. Radivojevic, PhD Thesis (2001)
[12] T. Martínez *et al.*, Nucl. Data Sheets, **120**, 78-80 (2014)
[13] K. Skrable *et al.*, Health Physics, **27**, 155-157 (1974)
[14] G. D'Agostini, Nucl. Instrum. and Methods A, **362**, 487-498 (1995)
[15] A. Pérez de Rada, PhD Thesis (2022)
[16] M. C. Brady, PhD Thesis (1989)